Computational Fluid Dynamics

Ex2

Almog Dobrescu

Table of Contents

List of Figures

Project Objective

Writing a general computer program to solve the Euler equations for a two-dimensional flow in curvilinear coordinates using the Beam & Warming algorithm (using the Euler implicit, first order temporal accuracy, scheme).

Governing Equations

Euler Equations

In two dimensions, the Euler equations take the form:

$$\frac{\partial Q}{\partial t}+\frac{\partial E}{\partial x}+\frac{\partial F}{\partial y}=0 \tag{1}$$

Where:

$$Q=\begin{pmatrix}\rho\\ \rho u\\ \rho v\\ e\end{pmatrix}, E=\begin{pmatrix}\rho u\\ \rho u^2+p\\ \rho uv\\ u(e+p)\end{pmatrix}, F=\begin{pmatrix}\rho v\\ \rho uv\\ \rho v^2+p\\ v(e+p)\end{pmatrix} \tag{2}$$

The generalized transformation in 2-D:

$$\begin{aligned} t&=\tau & \qquad \tau&=t\\ x&=x(\xi,\eta,\tau) & \qquad \xi&=\xi(x,y,t)\\ y&=y(\xi,\eta,\tau) & \qquad \eta&=\eta(x,y,t)\end{aligned} \tag{3}$$

The chain rule is given by:

$$\begin{pmatrix}\frac{\partial}{\partial t}\\ \frac{\partial}{\partial x}\\ \frac{\partial}{\partial y}\end{pmatrix}=\begin{pmatrix}1 & \xi_t & \eta_t\\ 0 & \xi_x & \eta_x\\ 0 & \xi_y & \eta_y\end{pmatrix}\cdot\begin{pmatrix}\frac{\partial}{\partial \tau}\\ \frac{\partial}{\partial \xi}\\ \frac{\partial}{\partial \eta}\end{pmatrix} \tag{4}$$

Applying the chain rule results in:

$$\frac{\partial Q}{\partial \tau}+\xi_t\frac{\partial Q}{\partial \xi}+\eta_t\frac{\partial Q}{\partial \eta}+\xi_x\frac{\partial E}{\partial \xi}+\eta_x\frac{\partial E}{\partial \eta}+\xi_y\frac{\partial F}{\partial \xi}+\eta_y\frac{\partial F}{\partial \eta}=0 \tag{5}$$

Multiply by J^{-1} and rewrite as follows:

$$(J^{-1}\xi_t Q)_\xi=Q(J^{-1}\xi_t)_\xi+J^{-1}\xi_t Q_\xi \tag{6}$$

Where J is the Jacobian

$$J=\xi_x\eta_y-\eta_x\xi_y=\frac{1}{x_\xi y_\eta-y_\xi x_\eta} \tag{7}$$

Applying the above relation on all terms:

$$\begin{aligned}&\left(\xi_t\frac{Q}{J}\right)_\xi - Q\left(\frac{\xi_t}{J}\right)_\xi + \left(\eta_t\frac{Q}{J}\right)_\eta - Q\left(\frac{\eta_t}{J}\right)_\eta + \left(\frac{Q}{J}\right)_\tau - Q\left(\frac{1}{J}\right)_\tau + \\ &+\left(\xi_x\frac{E}{J}\right)_\xi - E\left(\frac{\xi_x}{J}\right)_\xi + \left(\eta_x\frac{E}{J}\right)_\eta - E\left(\frac{\eta_x}{J}\right)_\eta + \\ &+\left(\xi_y\frac{F}{J}\right)_\xi - F\left(\frac{\xi_y}{J}\right)_\xi + \left(\eta_y\frac{F}{J}\right)_\eta - F\left(\frac{\eta_y}{J}\right)_\eta = 0\end{aligned} \tag{8}$$

Note:

$$\frac{\xi_x}{J} = y_\eta, \qquad \frac{\eta_x}{J} = -y_\xi, \qquad \frac{\xi_y}{J} = -x_\eta, \qquad \frac{\eta_y}{J} = x_\xi \tag{9}$$

Rearrange and substitute:

$$\begin{aligned}&-E\left(\frac{\xi_x}{J}\right)_\xi - E\left(\frac{\eta_x}{J}\right)_\eta - F\left(\frac{\xi_y}{J}\right)_\xi - F\left(\frac{\eta_y}{J}\right)_\eta = \\ &= -E\left(\left(y_\eta\right)_\xi - \left(y_\xi\right)_\eta\right) - F\left(\left(x_\xi\right)_\eta - \left(x_\eta\right)_\xi\right) \equiv 0\end{aligned} \tag{10}$$

Similarly:

$$-Q\left(\left(\frac{\xi_t}{J}\right)_\xi + \left(\frac{\eta_t}{J}\right)_\eta + \left(\frac{1}{J}\right)_\tau\right) \equiv 0 \tag{11}$$

The transformed equations therefore take the form:

$$\begin{gathered}\left(\frac{Q}{J}\right)_\tau + \left(\frac{\xi_t Q + \xi_x E + \xi_y F}{J}\right)_\xi + \left(\frac{\eta_t Q + \eta_x E + \eta_y F}{J}\right)_\eta = 0 \\ \frac{\partial \hat{Q}}{\partial \tau} + \frac{\partial \hat{E}}{\partial \xi} + \frac{\partial \hat{F}}{\partial \eta} = 0\end{gathered} \tag{12}$$

Where:

$$\hat{Q} = \frac{1}{J}\begin{pmatrix}\rho \\ \rho u \\ \rho v \\ e\end{pmatrix}$$

$$\hat{E} = \frac{1}{J}\begin{pmatrix}\xi_t\rho + \xi_x\rho u + \xi_y\rho v \\ \xi_t\rho u + \xi_x(p + \rho u^2) + \xi_y\rho uv \\ \xi_t\rho u + \xi_x\rho uv + \xi_y(e + pv^2) \\ \xi_t e + \xi_x(e + p)u + \xi_y(e + p)v\end{pmatrix} \tag{13}$$

$$\hat{F} = \frac{1}{J}\begin{pmatrix}\eta_t\rho + \eta_x\rho u + \eta_y\rho v \\ \eta_t\rho u + \eta_x(p + \rho u^2) + \eta_y\rho uv \\ \eta_t\rho u + \eta_x\rho uv + \eta_y(p + \rho v^2) \\ \eta_t e + \eta_x(e + p)u + \eta_y(e + p)v\end{pmatrix}$$

In our case, the mesh is fixed in time so:

$$\hat{Q} = \frac{1}{J}\begin{pmatrix} \rho \\ \rho u \\ \rho v \\ e \end{pmatrix}$$

$$\hat{E} = \frac{1}{J}\begin{pmatrix} \xi_x \rho u + \xi_y \rho v \\ \xi_x (p + \rho u^2) + \xi_y \rho u v \\ \xi_x \rho u v + \xi_y (e + p v^2) \\ \xi_x (e + p) u + \xi_y (e + p) v \end{pmatrix} \tag{14}$$

$$\hat{F} = \frac{1}{J}\begin{pmatrix} \eta_x \rho u + \eta_y \rho v \\ \eta_x (p + \rho u^2) + \eta_y \rho u v \\ \eta_x \rho u v + \eta_y (p + \rho v^2) \\ \eta_x (e + p) u + \eta_y (e + p) v \end{pmatrix}$$

Contravariant Velocities

The velocities in the computational coordinate direction, ξ and η:

$$\begin{matrix} U = \xi_t + \xi_x u + \xi_y v \\ V = \eta_t + \eta_x u + \eta_y v \end{matrix} \Rightarrow \begin{pmatrix} U \\ V \end{pmatrix} = \begin{pmatrix} \xi_x & \xi_y \\ \eta_x & \eta_y \end{pmatrix} \cdot \begin{pmatrix} u \\ v \end{pmatrix} \tag{15}$$

The inviscid rotated fluxes therefore take the form:

$$\hat{E} = \frac{1}{J}\begin{pmatrix} \rho U \\ \rho U u + \xi_x p \\ \rho U v + \xi_y p \\ (e + p) U - \xi_t p \end{pmatrix} \qquad \hat{F} = \frac{1}{J}\begin{pmatrix} \rho V \\ \rho V u + \eta_x p \\ \rho V v + \eta_y p \\ (e + p) V - \eta_t p \end{pmatrix} \tag{16}$$

The Numerical Scheme

Beam & Warming Algorithm

Utilize trapezoidal integration and forward differencing in time (second order in time):

$$\frac{\hat{Q}_{i,j}^{n+1} - \hat{Q}_{i,j}^{n}}{\Delta t} = -\frac{1}{2}\left(\frac{\partial \hat{E}_{i,j}^{n}}{\partial \xi} + \frac{\partial \hat{F}_{i,j}^{n}}{\partial \eta} + \frac{\partial \hat{E}_{i,j}^{n+1}}{\partial \xi} + \frac{\partial \hat{F}_{i,j}^{n+1}}{\partial \eta}\right) \tag{17}$$

Both E and F are non-linear functions of Q and therefore linearization is required prior to the evaluation of the spatial differences:

$$\begin{aligned} \hat{E}_{i,j}^{n+1} &= \hat{E}_{i,j}^{n} + \hat{A}_{i,j}^{n}\Delta\hat{Q}_{i,j}^{n} + high\ order\ terms \\ \hat{F}_{i,j}^{n+1} &= \hat{F}_{i,j}^{n} + \hat{B}_{i,j}^{n}\Delta\hat{Q}_{i,j}^{n} + high\ order\ terms \end{aligned} \tag{18}$$

Where:

$$\hat{A}_{i,j}^{n} \triangleq \frac{\partial \hat{E}_{i,j}^{n}}{\partial \hat{Q}_{i,j}^{n}} = \begin{pmatrix} 0 & \xi_x & \xi_y & 0 \\ \xi_x\phi^2 - u\theta_A & \theta_A - \xi_x\gamma_2 u & \xi_y u - \gamma_1\xi_x v & \xi_x\gamma_1 \\ \xi_y\phi^2 - v\theta_A & \xi_x v - \xi_y\gamma_1 u & \theta_A - \xi_y\gamma_2 v & \xi_y\gamma_1 \\ \theta_A\left(2\phi^2 - \frac{\gamma e}{\rho}\right) & \xi_x\beta - \gamma_1 u\theta_A & \xi_y\beta - \gamma_1 v\theta_A & \gamma\theta_A \end{pmatrix}$$

$$\hat{B}_{i,j}^{n} \triangleq \frac{\partial \hat{F}_{i,j}^{n}}{\partial \hat{Q}_{i,j}^{n}} = \begin{pmatrix} 0 & \eta_x & \eta_y & 0 \\ \eta_x\phi^2 - u\theta_B & \theta_B - \eta_x\gamma_2 u & \eta_y u - \gamma_1\eta_x v & \eta_x\gamma_1 \\ \eta_y\phi^2 - v\theta_B & \eta_x v - \eta_y\gamma_1 u & \theta_B - \eta_y\gamma_2 v & \eta_y\gamma_1 \\ \theta_B\left(2\phi^2 - \frac{\gamma e}{\rho}\right) & \eta_x\beta - \gamma_1 u\theta_B & \eta_y\beta - \gamma_1 v\theta_B & \gamma\theta_B \end{pmatrix} \tag{19}$$

$$\begin{aligned} \phi^2 &= \tfrac{1}{2}(\gamma - 1)(u^2 + v^2) \\ \theta_A &= \xi_x u + \xi_y v \\ \theta_B &= \eta_x u + \eta_y v \\ \gamma_1 &= \gamma - 1 \\ \gamma_2 &= \gamma - 2 \\ \beta &= \frac{\gamma e}{\rho} - \phi^2 \\ \Delta\hat{Q}_{i,j}^{n} &\triangleq \hat{Q}_{i,j}^{n+1} - \hat{Q}_{i,j}^{n} \end{aligned} \tag{20}$$

Applying the Taylor series expansion:

$$\begin{aligned} \frac{\partial \hat{E}_{i,j}^{n+1}}{\partial \xi} &= \frac{\partial \hat{E}_{i,j}^{n}}{\partial \xi} + \frac{\partial}{\partial \xi}\left(\hat{A}_{i,j}^{n}\Delta\hat{Q}_{i,j}^{n}\right) \\ \frac{\partial \hat{F}_{i,j}^{n+1}}{\partial \eta} &= \frac{\partial \hat{F}_{i,j}^{n}}{\partial \eta} + \frac{\partial}{\partial \eta}\left(\hat{B}_{i,j}^{n}\Delta\hat{Q}_{i,j}^{n}\right) \end{aligned} \tag{21}$$

Therefore:

$$\frac{1}{2}\left(\frac{\partial \hat{E}_{i,j}^{n}}{\partial \xi}+\frac{\partial \hat{E}_{i,j}^{n+1}}{\partial \xi}\right)=\frac{\partial \hat{E}_{i,j}^{n}}{\partial \xi}+\frac{1}{2}\frac{\partial}{\partial \xi}\left(\hat{A}_{i,j}^{n}\Delta \hat{Q}_{i,j}^{n}\right)$$
$$\frac{1}{2}\left(\frac{\partial \hat{F}_{i,j}^{n}}{\partial \eta}+\frac{\partial \hat{F}_{i,j}^{n+1}}{\partial \eta}\right)=\frac{\partial \hat{F}_{i,j}^{n}}{\partial \eta}+\frac{1}{2}\frac{\partial}{\partial \eta}\left(\hat{B}_{i,j}^{n}\Delta \hat{Q}_{i,j}^{n}\right) \tag{22}$$

Substitution of the Taylor series expansion results in (delta form):

$$\underbrace{\left(I+\frac{\Delta t}{2}\left(\frac{\partial \hat{A}_{i,j}^{n}}{\partial \xi}+\frac{\partial \hat{B}_{i,j}^{n}}{\partial \eta}\right)\right)}_{\text{LHS}}\cdot \Delta \hat{Q}_{i,j}^{n}=\underbrace{-\Delta t\left(\frac{\partial \hat{E}_{i,j}^{n}}{\partial \xi}+\frac{\partial \hat{F}_{i,j}^{n}}{\partial \eta}\right)}_{\text{RHS}} \tag{23}$$

The first order implicit Euler scheme is given by:

$$\underbrace{\left(I+\Delta t\left(\frac{\partial \hat{A}_{i,j}^{n}}{\partial \xi}+\frac{\partial \hat{B}_{i,j}^{n}}{\partial \eta}\right)\right)}_{\text{LHS}}\cdot \Delta \hat{Q}_{i,j}^{n}=\underbrace{-\Delta t\left(\frac{\partial \hat{E}_{i,j}^{n}}{\partial \xi}+\frac{\partial \hat{F}_{i,j}^{n}}{\partial \eta}\right)}_{\text{RHS}} \tag{24}$$

Beam and Warming uses central differencing for the spatial derivative approximations, resulting in (implicit Euler):

$$\underbrace{\left(I+\Delta t\left(\frac{D_{0_\xi}\hat{A}_{i,j}^{n}}{2\Delta \xi}+\frac{D_{0_\eta}\hat{B}_{i,j}^{n}}{2\Delta \eta}\right)\right)}_{\text{LHS}}\cdot \Delta \hat{Q}_{i,j}^{n}=\underbrace{-\Delta t\left(\frac{D_{0_\xi}\hat{E}_{i,j}^{n}}{2\Delta \xi}+\frac{D_{0_\eta}\hat{F}_{i,j}^{n}}{2\Delta \eta}\right)}_{\text{RHS}} \tag{25}$$

Where:

$$D_{0_\xi}f_{i,j}=f_{i+1,j}-f_{i-1,j}$$
$$and \tag{26}$$
$$D_{0_\eta}f_{i,j}=f_{i,j+1}-f_{i,j-1}$$

After applying artificial smoothing:

$$\underbrace{\left(I+\Delta t\left(\frac{D_{0_\xi}\hat{A}_{i,j}^{n}}{2\Delta \xi}+\frac{D_{0_\eta}\hat{B}_{i,j}^{n}}{2\Delta \eta}+D_{is_\xi}+D_{is_\eta}\right)\right)}_{\text{LHS}}\cdot \Delta \hat{Q}_{i,j}^{n}$$
$$=\underbrace{-\Delta t\left(\frac{D_{0_\xi}\hat{E}_{i,j}^{n}}{2\Delta \xi}+\frac{D_{0_\eta}\hat{F}_{i,j}^{n}}{2\Delta \eta}\right)+D_{es_\xi}Q^{n}+D_{es_\eta}Q^{n}}_{\text{RHS}} \tag{27}$$

The implicit scheme requires inversion of a block penta-diagonal matrix with $4x4$ blocks (block hepta-diagonal matrix with $5x5$ blocks in 3-D). The required inversion is costly and therefore approximate factorization is applied as follows (implicit Euler):

$$\left(I + \Delta t \frac{D_{0_\xi} \hat{A}^n_{i,j}}{2\Delta\xi} + \Delta t D_{is_\xi}\right)\left(I + \Delta t \frac{D_{0_\eta} \hat{B}^n_{i,j}}{2\Delta\eta} + \Delta t D_{is_\eta}\right)\Delta\hat{Q}^n_{i,j} = RHS^n_{i,j} \tag{28}$$

In our case:

$$\Delta\xi = 1 \qquad and \qquad \Delta\eta = 1 \tag{29}$$

Beam & Warming – Solution Procedure

Define:

$$\left(I + \frac{\Delta t}{2} D_{0_\eta} \hat{B}^n_{i,j} + \Delta t D_{is_\eta}\right)\Delta\hat{Q}^n_{i,j} \triangleq \Delta\hat{Q}^{n\,*}_{i,j} \tag{30}$$

Solve:

$$\left(I + \frac{\Delta t}{2} D_{0_\xi} \hat{A}^n_{i,j} + \Delta t D_{is_\xi}\right)\Delta\hat{Q}^{n\,*}_{i,j} = RHS^n_{i,j} \tag{31}$$

Solve:

$$\left(I + \frac{\Delta t}{2} D_{0_\eta} \hat{B}^n_{i,j} + \Delta t D_{is_\eta}\right)\Delta\hat{Q}^n_{i,j} \triangleq \Delta\hat{Q}^{n\,*}_{i,j} \tag{32}$$

Advance:

$$\hat{Q}^{n+1}_{i,j} = \hat{Q}^n_{i,j} + \Delta\hat{Q}^n_{i,j} \tag{33}$$

Returning to the physical domain:

$$Q^{n+1}_{i,j} = Q_{i,j} + \Delta\hat{Q}^n_{i,j} \cdot J_{i,j} \tag{34}$$

Each factor is a series of block tridiagonal line inversions, e.g. the ξ coordinate direction linear system:

$$\begin{pmatrix} I & \frac{\Delta t}{2}\hat{A}^n_2 & 0 & \dots & \dots \\ -\frac{\Delta t}{2}\hat{A}^n_1 & I & \frac{\Delta t}{2}\hat{A}^n_3 & 0 & \dots \\ 0 & \ddots & \ddots & \ddots & 0 \\ \dots & 0 & -\frac{\Delta t}{2}\hat{A}^n_{k-2} & I & \frac{\Delta t}{2}\hat{A}^n_k \\ \dots & \dots & 0 & -\frac{\Delta t}{2}\hat{A}^n_{k-1} & I \end{pmatrix}\begin{pmatrix} \Delta\hat{Q}^{n\,*}_1 \\ \Delta\hat{Q}^{n\,*}_2 \\ \dots \\ \dots \\ \dots \\ \dots \\ \Delta\hat{Q}^{n\,*}_{k-1} \\ \Delta\hat{Q}^{n\,*}_k \end{pmatrix} = \begin{pmatrix} RHS^n_1 \\ RHS^n_2 \\ \dots \\ \dots \\ \dots \\ \dots \\ RHS^n_{k-1} \\ RHS^n_k \end{pmatrix} \tag{35}$$

The η coordinate direction linear system:

$$\begin{pmatrix} I & \frac{\Delta t}{2}\hat{B}_2^n & 0 & \dots & \dots \\ -\frac{\Delta t}{2}\hat{B}_1^n & I & \frac{\Delta t}{2}\hat{B}_3^n & 0 & \dots \\ 0 & \ddots & \ddots & \ddots & 0 \\ \dots & 0 & -\frac{\Delta t}{2}\hat{B}_{k-2}^n & I & \frac{\Delta t}{2}\hat{B}_k^n \\ \dots & \dots & 0 & -\frac{\Delta t}{2}\hat{B}_{k-1}^n & I \end{pmatrix} \begin{pmatrix} \Delta\hat{Q}_1^n \\ \Delta\hat{Q}_2^n \\ \dots \\ \dots \\ \dots \\ \Delta\hat{Q}_{k-1}^n \\ \Delta\hat{Q}_k^n \end{pmatrix} = \begin{pmatrix} \Delta\hat{Q}_1^{n^*} \\ \Delta\hat{Q}_2^{n^*} \\ \dots \\ \dots \\ \dots \\ \Delta\hat{Q}_{k-1}^{n^*} \\ \Delta\hat{Q}_k^{n^*} \end{pmatrix} \tag{36}$$

Convergence Condition

The convergence criterion is the norm of $\Delta\hat{Q}_{i,j}^n$.

When $\Delta\hat{Q}_{i,j}^n$ drops 6 orders of magnitude, the solution is considered converged.

Boundary Conditions – Implementation on a Computational Mesh

Wall BC

Inviscid flow, adiabatic wall boundary conditions in 2-D – Finite differences:

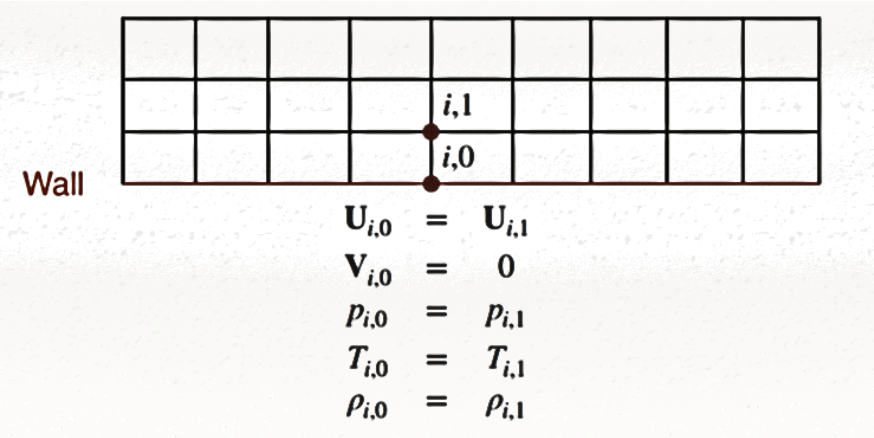

Figure 1: Wall BC

$$\begin{cases} U_{i,0} = U_{i,1} \\ V_{i,0} = 0 \end{cases} \Rightarrow \begin{cases} \xi_{x_{i,0}}u_{i,0} + \xi_{y_{i,0}}v_{i,0} = \xi_{x_{i,1}}u_{i,1} + \xi_{y_{i,1}}v_{i,1} \\ \eta_{x_{i,0}}u_{i,0} + \eta_{y_{i,0}}v_{i,0} = 0 \end{cases} \tag{37}$$

Isolating $u_{i,0}$ and $v_{i,0}$:

$$\begin{cases} u_{i,0} = U_{i,1} \cdot \dfrac{\eta_{y_{i,0}}}{J_{i,0}} \\ v_{i,0} = -U_{i,1} \cdot \dfrac{\eta_{x_{i,0}}}{J_{i,0}} \end{cases} \tag{38}$$

$$\rho_{i,0} = \rho_{i,1} \tag{39}$$

$$p_{i,0} = p_{i,1} = (\gamma - 1)\left(e_{i,1} - \frac{1}{2}\rho_{i,1}\left(u_{i,1}^2 + v_{i,1}^2\right)\right) \tag{40}$$

$$e_{i,0} = \frac{p_{i,0}}{\gamma - 1} + \frac{1}{2}\rho_{i,0}\left(u_{i,0}^2 + v_{i,0}^2\right) \tag{41}$$

Trailing Edge BC

Applying the Kutta condition:

$$p_{i_{teu},0} = (\gamma - 1)\left(e_{i_{teu},0} - \frac{1}{2}\rho_{i_{teu},0}\left(u_{i_{teu},0}^2 + v_{i_{teu},0}^2\right)\right) \tag{42}$$

$$p_{i_{tel},0} = (\gamma - 1)\left(e_{i_{tel},0} - \frac{1}{2}\rho_{i_{tel},0}\left(u_{i_{tel},0}^2 + v_{i_{tel},0}^2\right)\right) \tag{43}$$

$$\begin{aligned} p_{i_{te},0} &= \frac{1}{2}\left(p_{i_{teu},0} + p_{i_{tel},0}\right) \\ u_{i_{te},0} &= \frac{1}{2}\left(u_{i_{teu},0} + u_{i_{tel},0}\right) \\ v_{i_{te},0} &= \frac{1}{2}\left(v_{i_{teu},0} + v_{i_{tel},0}\right) \\ \rho_{i_{te},0} &= \frac{1}{2}\left(\rho_{i_{teu},0} + \rho_{i_{tel},0}\right) \end{aligned} \tag{44}$$

$$e_{i_{te},0} = \frac{p_{i_{te},0}}{\gamma - 1} + \frac{1}{2}\rho_{i_{te},0}\left(u_{i_{te},0}^2 + v_{i_{te},0}^2\right) \tag{45}$$

$$\Downarrow$$

$$Q_{i_{te},0} = \begin{pmatrix} \rho_{i_{te},0} \\ \rho_{i_{te},0} \cdot u_{i_{te},0} \\ \rho_{i_{te},0} \cdot v_{i_{te},0} \\ e_{i_{te},0} \end{pmatrix} \tag{46}$$

Cut BC

Applying simple averaging of the Q vector along the wake:

$$Q_{i,0} = \frac{1}{2}\left(Q_{i,1} + Q_{ni-1-i,1}\right) \tag{47}$$

$$Q_{ni-1-i,0} = Q_{i,0} \tag{48}$$

Outflow

Applying simple extrapolation:

$$\begin{aligned} Q_{0,j} &= Q_{i,j} \\ Q_{ni-1,j} &= Q_{ni-2,j} \end{aligned} \tag{49}$$

Functional Description

Flow Chart

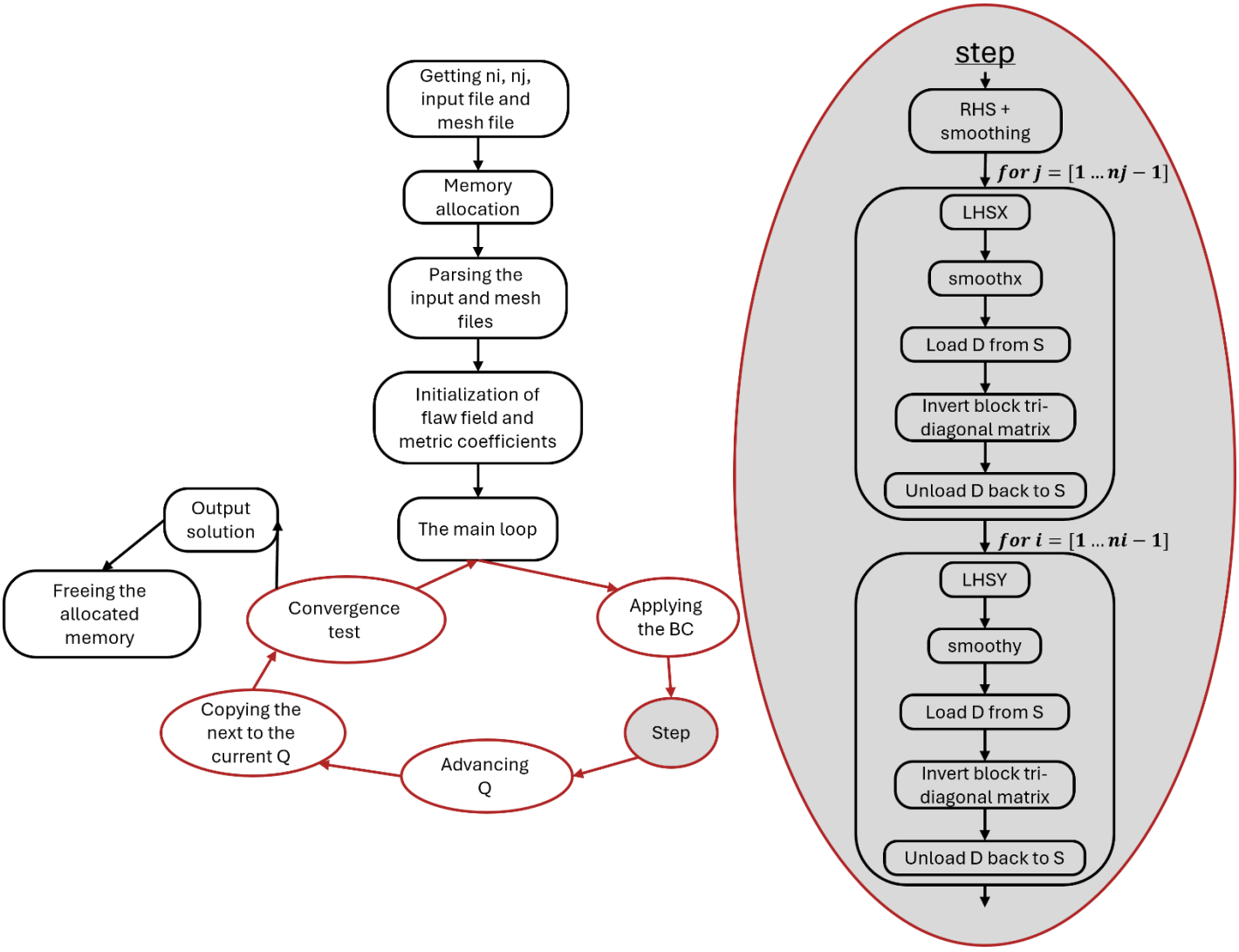

The functions in the program

The functions that are included in the program and explanation about them are included in the code itself.

Results

$M_\infty = 0.9$

Flow field

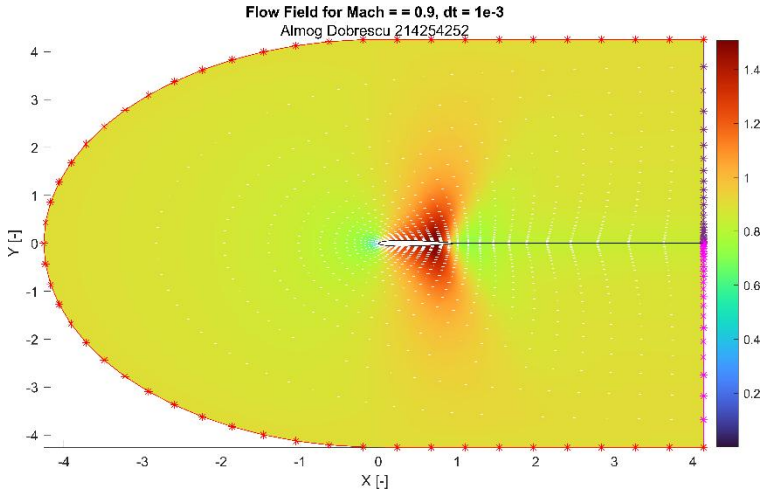

Figure 2: Flow field for $M_\infty = 0.9$

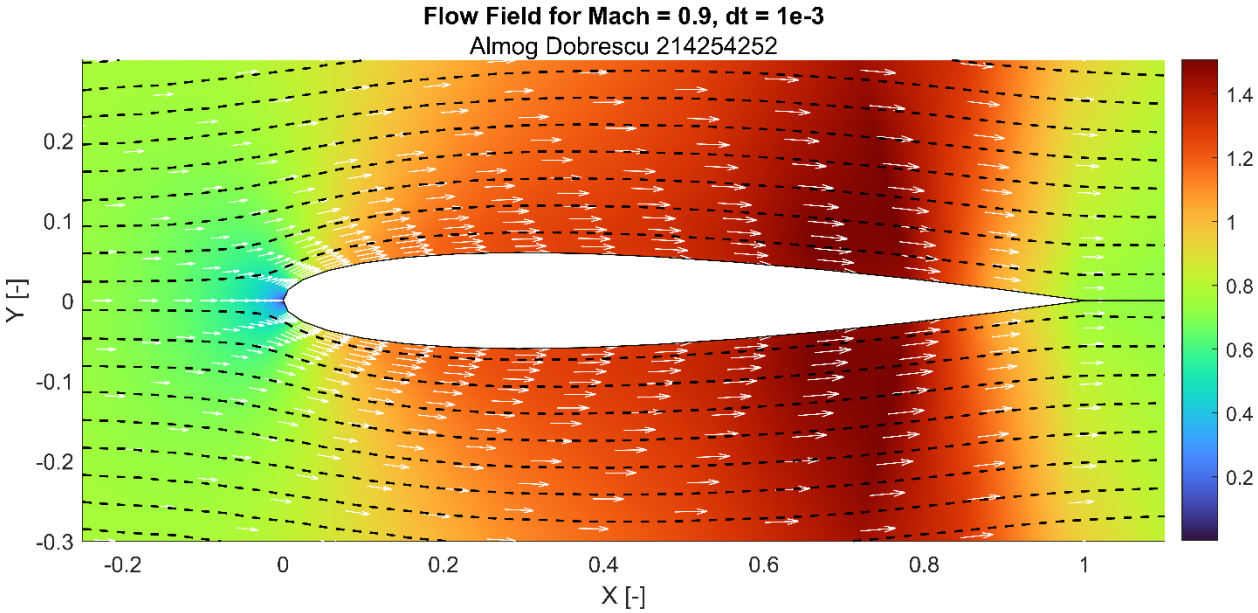

Figure 3: Flow field for $M_\infty = 0.9$ - zoom

We can see that an expansion fan is forming near the trailing edge and the flow field is symmetric

Convergence history

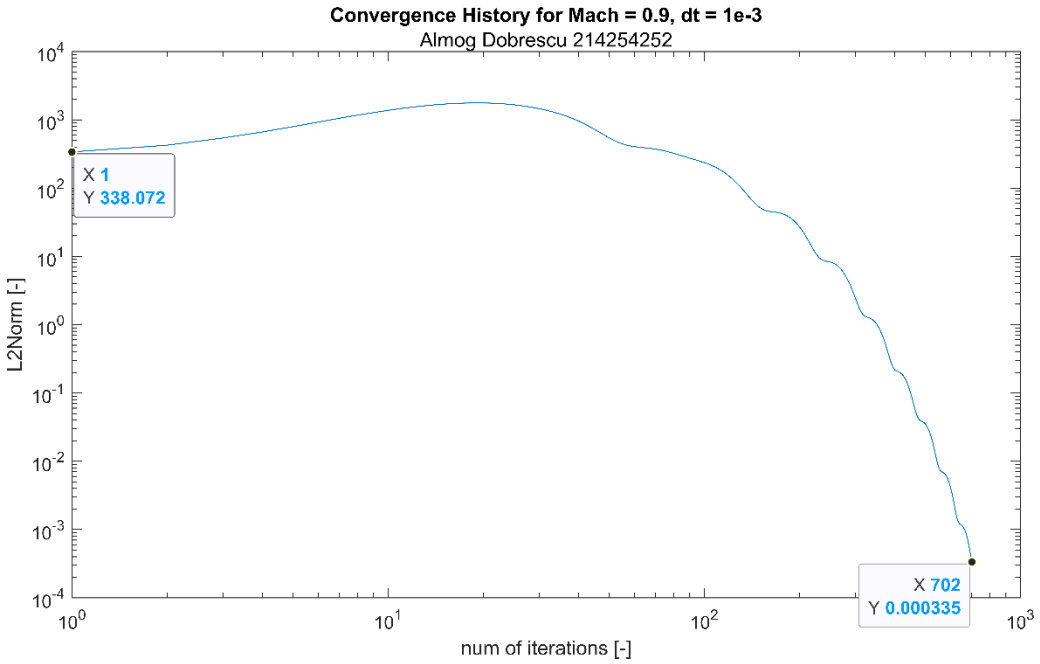

Figure 4: Convergence history for $M_\infty = 0.9$

We can see that at first the flow field changes rapidly and slowly start to stabilize around a solution. In this case, it took 702 iterations before L2Norm drops 6 orders of magnitude.

Mach distribution on the airfoil

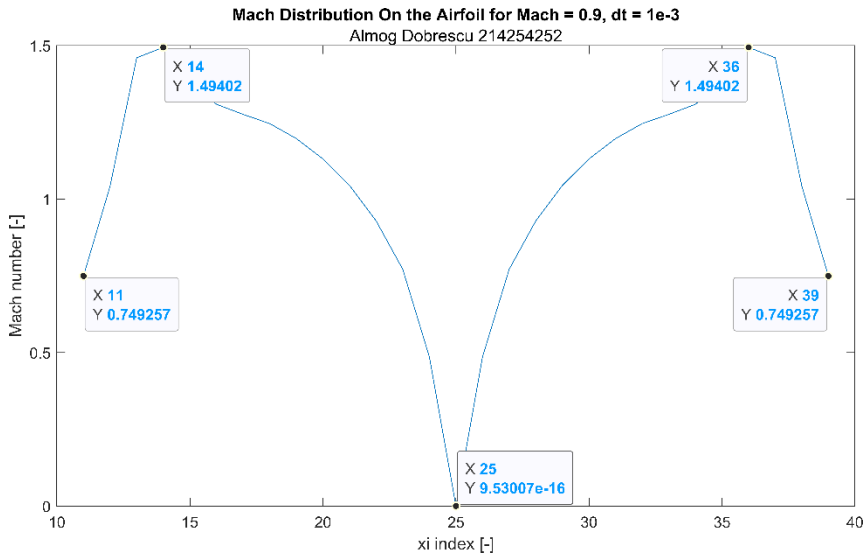

Figure 5: Mach distribution on the airfoil for $M_\infty = 0.9$

We can see that the Mach distribution is symmetric around the leading edge, as expected because the angle of attack is zero. Moreover, the Mach number at the trailing edge is lower than at infinity.

Pressure distribution on the airfoil

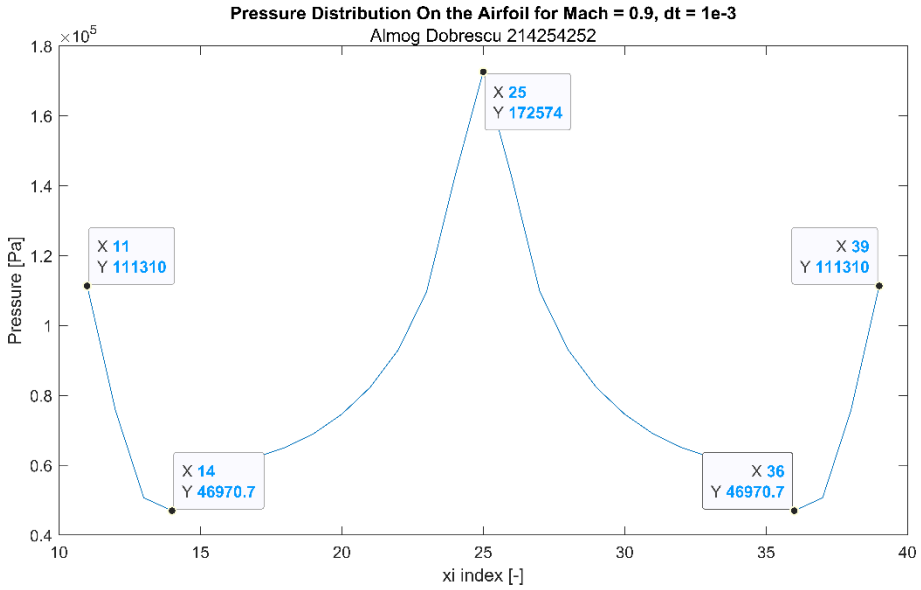

Figure 6: Pressure distribution on the airfoil for $M_\infty = 0.9$

We can see that the pressure distribution is symmetric around the leading edge, as expected because the angle of attack is zero. Moreover, the pressure distribution is exactly inverse to the Mach distribution and the maximal pressure is at the leading edge.

$M_\infty = 1.5$

Flow field

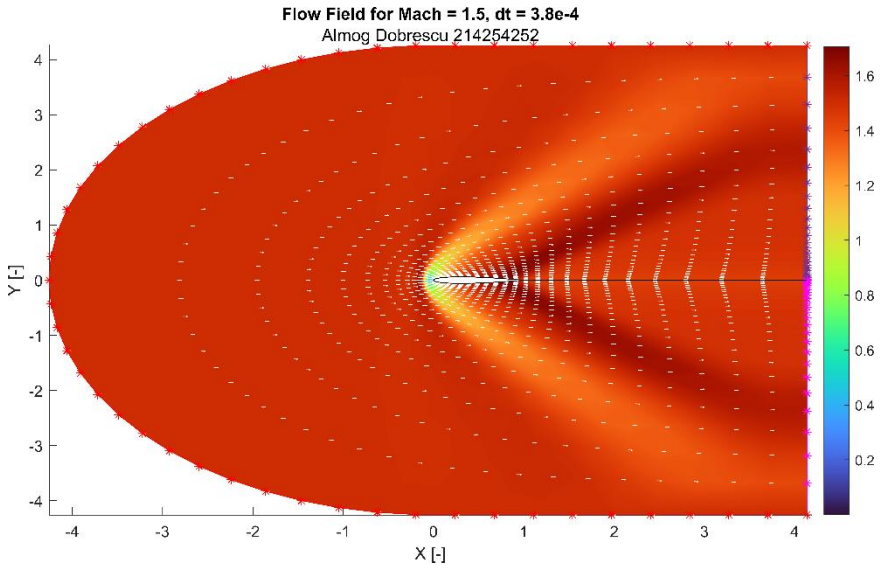

Figure 7: Flow field for $M_\infty = 1.5$

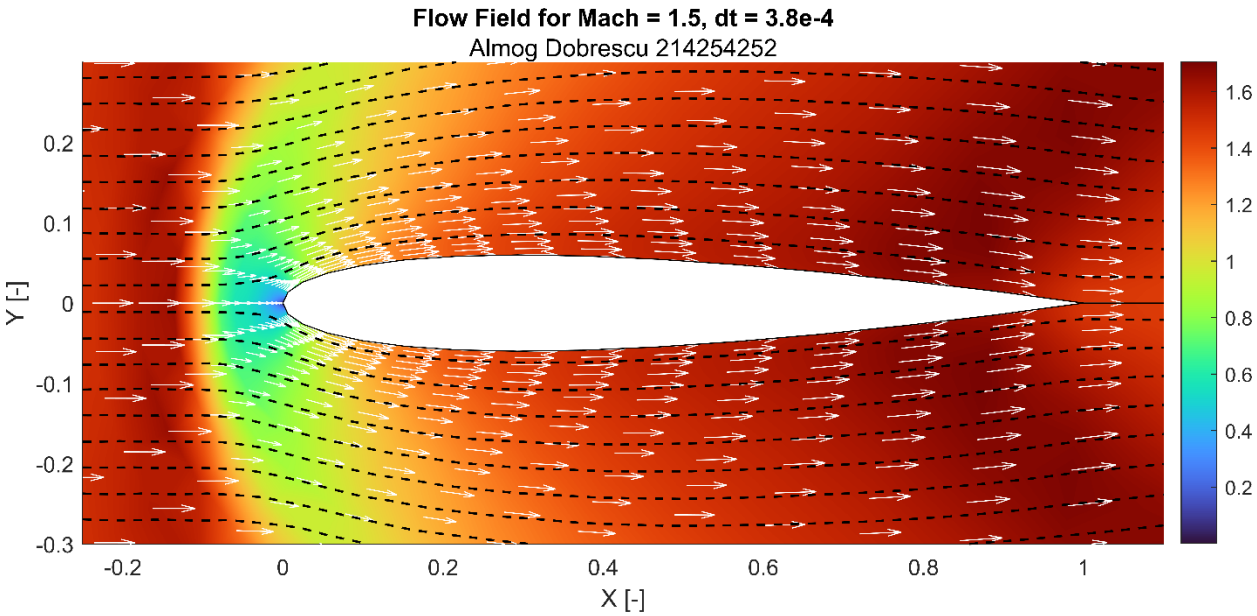

Figure 8: Flow field for $M_\infty = 1.5$ - zoom

We can see a detached shock wave in front of the leading edge of the airfoil. Moreover, the angle of the expansion fan near the trailing edge is smaller in comparison to the expansion fan in $M_\infty = 0.9$ seen in Figure 3.

Convergence history

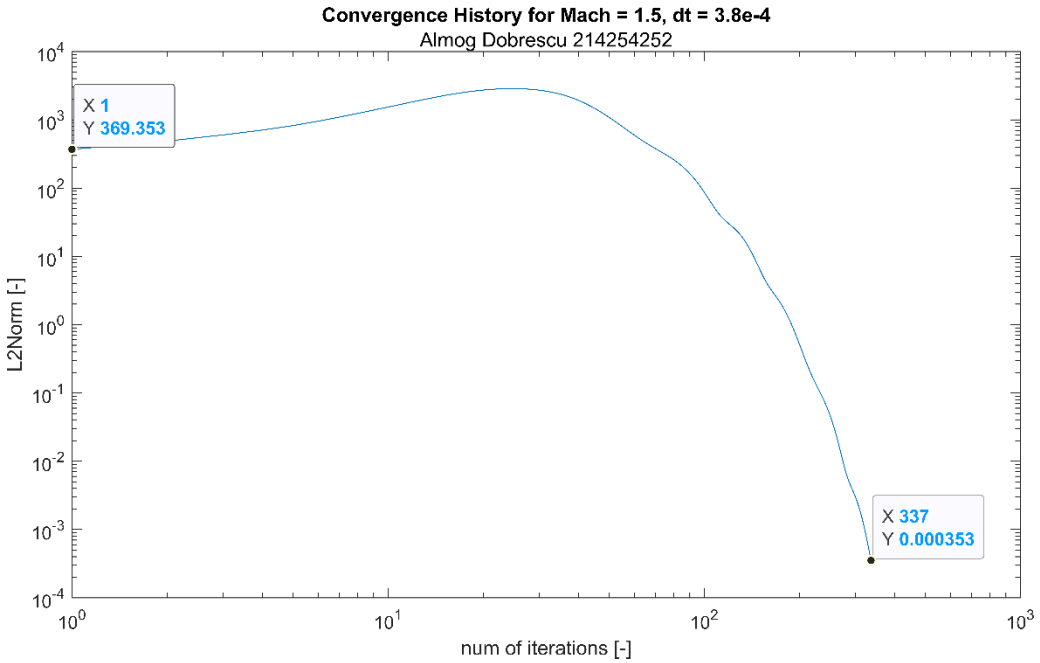

Figure 9: Convergence history for $M_\infty = 1.5$

We can see that at first the flow field changes rapidly and slowly start to stabilize around a solution. In this case, it took 339 iterations before L2Norm drops 6 orders of magnitude.

Mach distribution on the airfoil

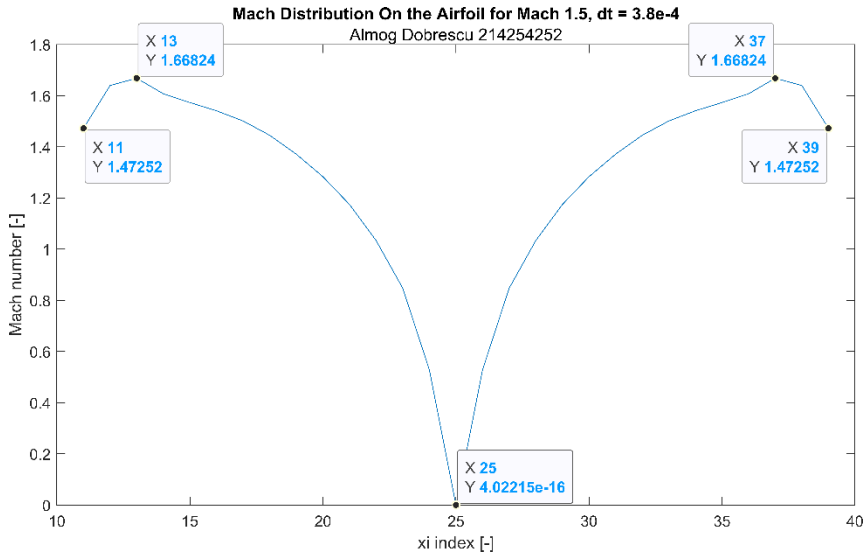

Figure 10: Mach distribution on the airfoil for $M_\infty = 1.5$

We can see that the Mach distribution is symmetric around the leading edge, as expected because the angle of attack is zero. Moreover, the Mach number at the trailing edge is lower than at infinity.

Pressure distribution on the airfoil

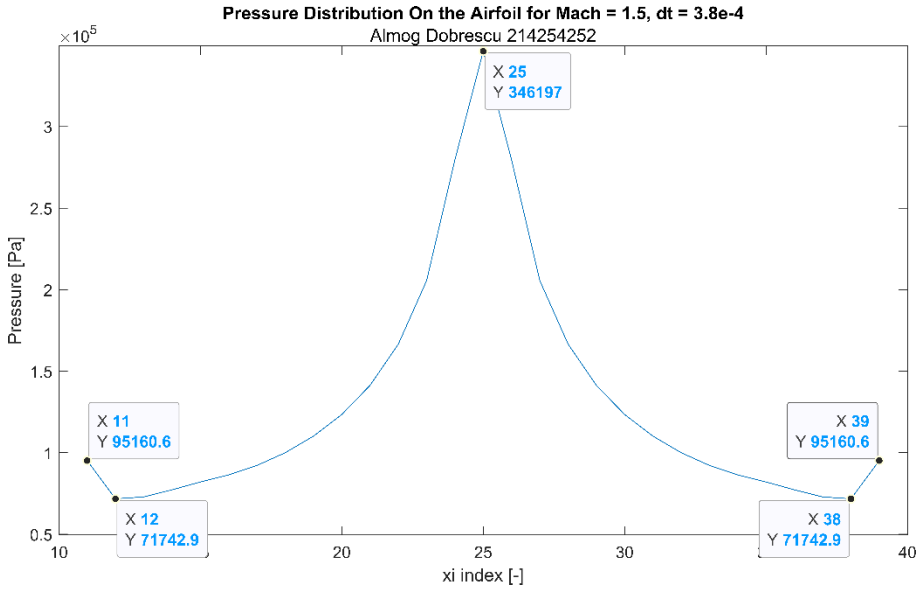

Figure 11: Pressure distribution on the airfoil for $M_\infty = 1.5$

We can see that the pressure distribution is symmetric around the leading edge, as expected because the angle of attack is zero. Moreover, the pressure distribution is almost exactly inverse to the Mach distribution and the maximal pressure is at the leading edge.

Effect of Time Step on Results for $M = 0.9$

Convergence History

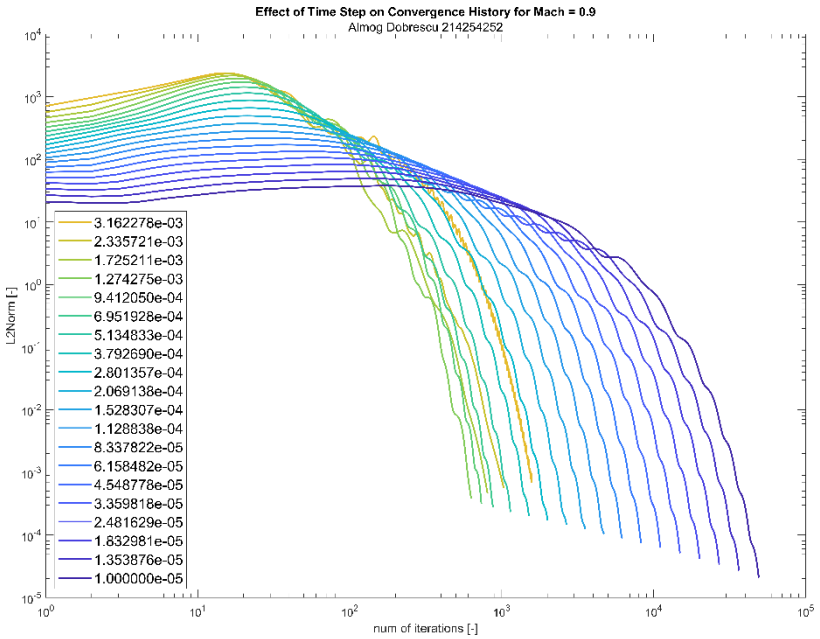

Figure 12: Effect of time step on convergence history for $M = 0.9$

We can see that there is an optimal Δt for whom the number of iterations is minimal.

Below that Δt the solver becomes quite unstable.

Mach distribution on the airfoil

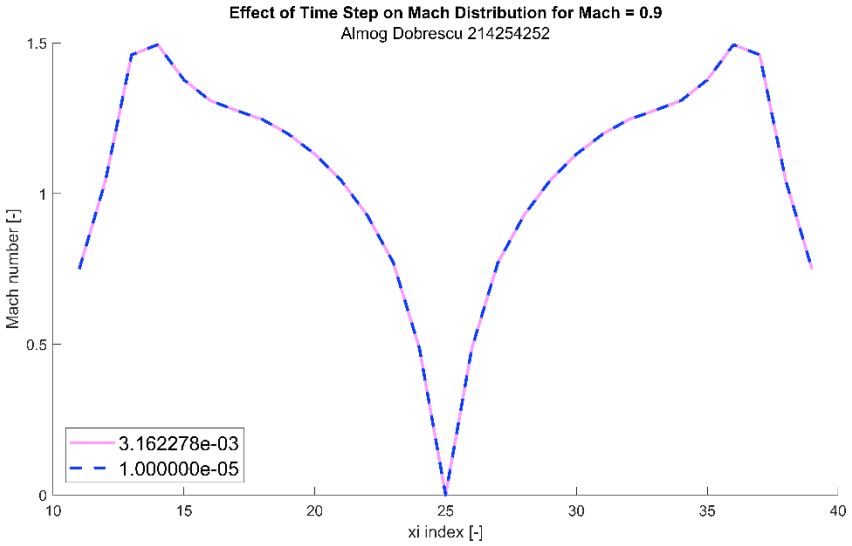

Figure 13: Effect of time step on Mach distribution for $M = 0.9$

We can see that there is no difference in the Mach distribution on the airfoil for difference Δt.

Pressure distribution on the airfoil

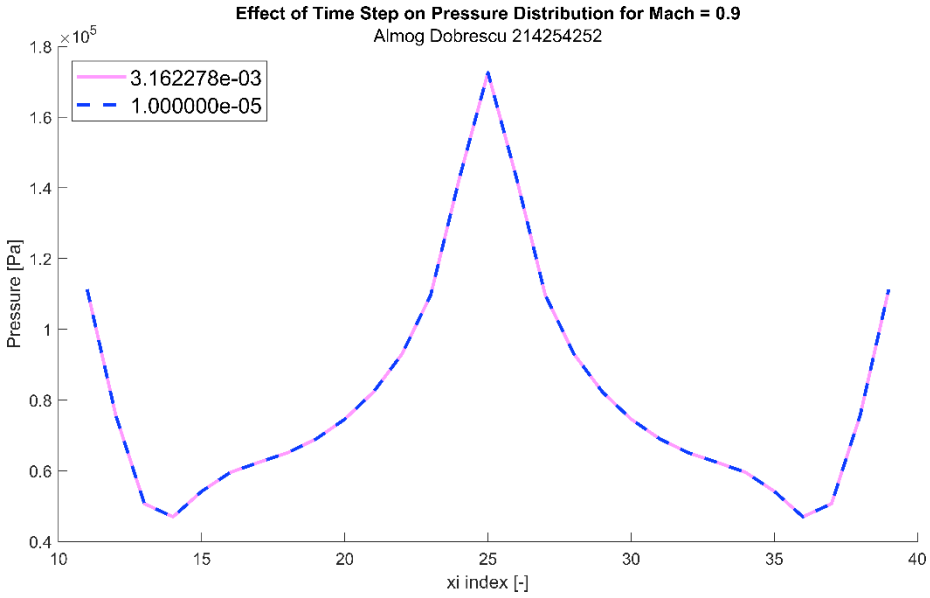

Figure 14: Effect of time step on pressure distribution for $M = 0.9$

We can see that there is no difference in the pressure distribution on the airfoil for difference Δt.

Effect of Time Step on Results for $M = 1.5$

Convergence History

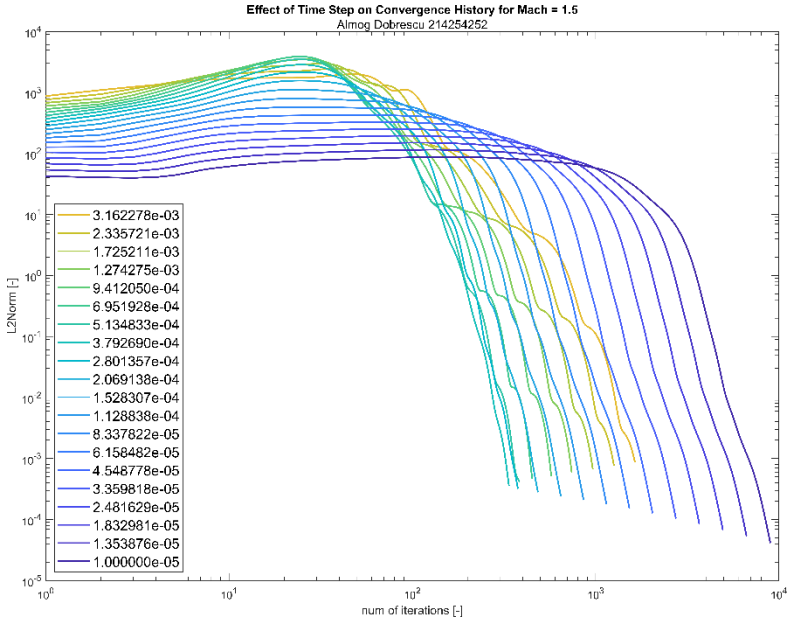

Figure 15: Effect of time step on convergence history for $M = 1.5$

We can see that there is an optimal Δt for whom the number of iterations is minimal.

Below that Δt the solver becomes quite unstable.

Mach distribution on the airfoil

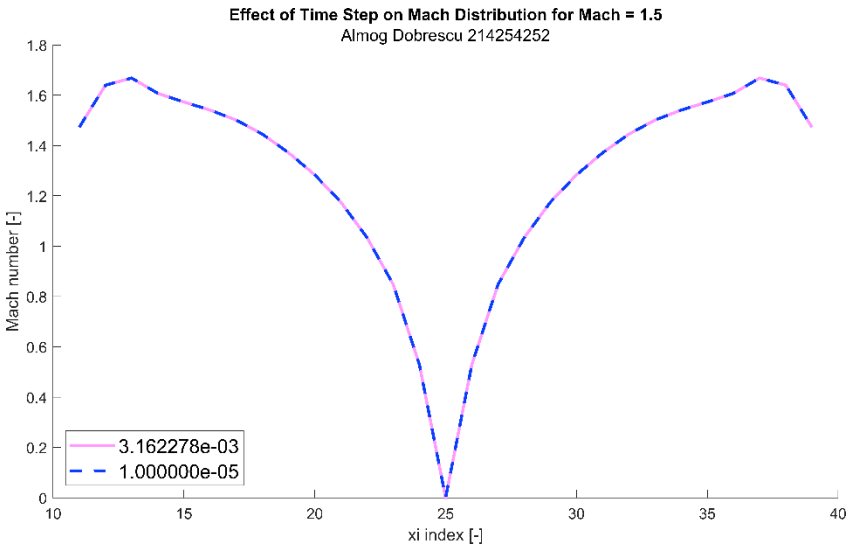

Figure 16: Effect of time step on Mach distribution for $M = 1.5$

We can see that there is no difference in the Mach distribution on the airfoil for difference Δt.

Pressure distribution on the airfoil

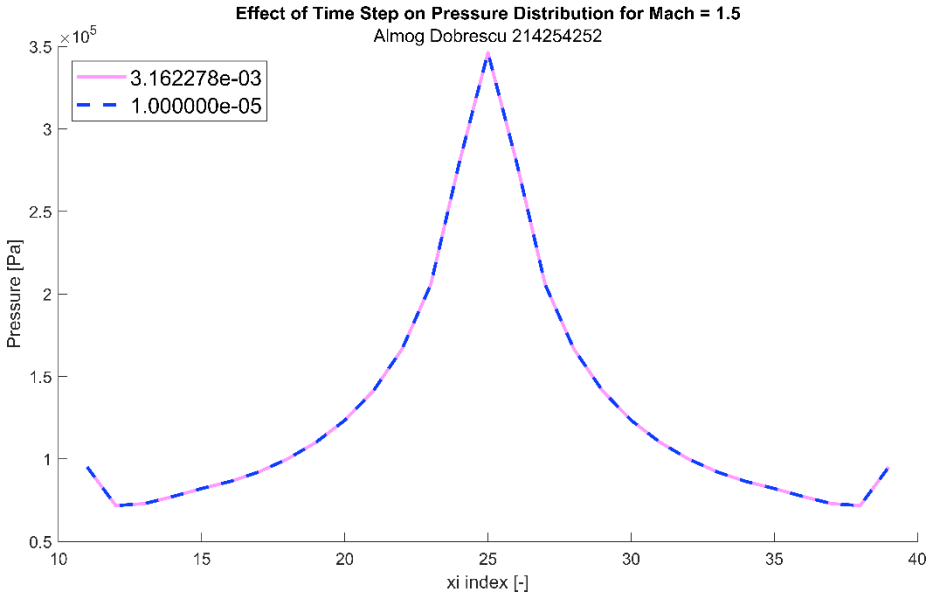

Figure 17: Effect of time step on pressure distribution for $M = 1.5$

We can see that there is no difference in the pressure distribution on the airfoil for difference Δt.

Conclusions

- The time step, Δt, does not change the final qualitative and quantitative results (in the range of $\Delta t \in [10^{-5} \dots 10^{-2.5}]$, for $M_\infty \in [0.9, 1.5]$), as seen in Figure 13, Figure 14, Figure 16 and Figure 17.
- For different M_∞ values, there is a different optimal Δt for minimal number of iterations, as shown in Figure 12 and Figure 15.
- The pressure and the Mach number are anti-symmetric to each other. This fact can be observed in the pairs of figures: Figure 5, Figure 6 and Figure 10, Figure 11.
- When the angel of attack is zero, the velocity (Mach number) is indeed zero at the leading edge. It can be clearly seen in Figure 3 and Figure 8.
- As the M_∞ grows, the solver can "handle" bigger time steps (Δt) as seen in the differences between figures Figure 12 and Figure 15.
- As M_∞ grows, the expansion fan occurs later (closer to the trailing edge). This can be seen in the difference between Figure 5 and Figure 10